PREPRINT

Title: RESPONSE OF TENSION PILES TO SIMULATED SEISMIC MOTION IN SATURATED FINE SAND

Author(s): Michael W. O'Neill,

Cumaraswamy Vipulanandan

and Mauricio Ochoa

RESPONSE OF TENSION PILES TO SIMULATED SEISMIC MOTION IN SATURATED FINE SAND

by

Michael W. O'Neill[1], Cumaraswamy Vipulanandan[1] and Mauricio Ochoa[2]

ABSTRACT

A laboratory model study of tension piles subjected to simulated seismic loading through the soil was conducted. The objective of the study was to assess the magnitude of biased (static) tension load that can be sustained by displacement-type piles driven into medium dense, saturated fine sand during seismic events typical of those in Southern California. The prototype pile characteristics modeled in this study consisted of a closed-end, or plugged, impact-driven pipe pile, 20 to 40 in. in diameter, 20 to 40 ft in length (or top 20 to 40 ft of a longer pile). An acceleration record for a particular Magnitude 5.8 seismic event, the Oceanside earthquake of July 13, 1986, measured at an offshore (California) deep soil site, 45 mi. (74 km) from the epicenter, was selected and scaled to higher magnitudes to simulate more severe earthquake loading conditions on the pile.

A 21-inch-high by 20-inch-diameter pressure chamber was used to contain the saturated soil and to simulate isotropic effective stresses and drainage conditions. The model test pile was an instrumented, steel, closed-end tube, 1 inch in diameter and 16 inches long, that was loaded through a spring-mass system to simulate feedback from a simple superstructure with a known natural period. Pile-head movements, pile load vs. depth and pore water pressures in the soil were measured during the experiments. Both the simulated seismic record and/or soil permeability were scaled to model the effect of drainage distance and its effect on pore water pressure generation and dissipation.

---

[1] Department of Civil and Environmental Engineering, University of Houston, Houston, TX 77204-4791

[2] McBride-Ratcliff and Assoc., 7220 Langtry, Houston, TX 77040

Contour plots of stability conditions (sustained tension resistance and small pile movements), mobility conditions (sustained resistance associated with substantial pile movements) and failure conditions (total loss of pile capacity) for the model pile were developed from the tests. The effect of distance between the pile and event epicenter on stability was considered analytically.

RESPONSE OF TENSION PILES TO SIMULATED SEISMIC MOTION IN SATURATED FINE SAND

by

Michael W. O'Neill[1], Cumaraswamy Vipulanandan[1] and Mauricio Ochoa[2]

INTRODUCTION

A laboratory study of tension piles in submerged, fine sand that are subjected to simulated seismic loading has been conducted in order to assess the magnitude of biased (static) tension load that can be sustained by displacement-type piles. Biased tension loads may be present on piles that support structures subjected to large static overturning moments, including hydraulic structures and bridges; tension-leg offshore platforms; and pile-anchored floating bridges. The prototype pile characteristics modeled in this study consisted of a closed-end, impact-driven pile, 20 to 40 in. in diameter, 20 to 40 feet in length (or top 20 to 40 feet of a longer pile), and driven in a fine, uniform, clean siliceous sand at relative densities ranging from 55% to 70%. These relative densities were selected to represent the range for medium dense sand. Values biased toward the high side of the normal range for medium dense sands (33% - 67%) were used because the test sand was not aged and would behave similar to aged prototype sand at relative densities lower than that of the test sand.

The soil-pile model system was excited so as to simulate the vertical, horizontal and combined vertical and horizontal components of an earthquake at a deep soil site that is under water. The rationale that dictated the investigation was that the interaction of the excited soil and the pile would induce shearing stresses at the interface of the soil and pile, which, along with the stress waves in the soil itself, would produce excess pore water

---

[1] Department of Civil and Environmental Engineering, University of Houston, Houston, TX 77204-4791

[2] McBride-Ratcliff and Assoc., 7220 Langtry, Houston, TX 77040

pressures, and perhaps reductions in effective stress at the pile wall due to grain reorientation in the sand. Such phenomena would reduce the uplift capacity of the pile and either cause the pile to pull out under a biased tension load lower than its static axial capacity or produce a permanent post-event reduction in uplift capacity. The practical problem that originally motivated the study was concern for the stability of pile foundations for tension-leg offshore platforms. The results are equally applicable to floating bridge foundations in deep water, however.

MODELLING

Event Selection

The phenomenon was studied by selecting a particular seismic event in which acceleration time histories had been measured at an offshore deep soil site. The event chosen for study was the Oceanside, California, event of July 13, 1986 ([1]), a Magnitude 5.8 earthquake whose epicenter was 45 mi. (74 km) southeast of the instrumentation site. Accelerations were measured on the shallow sea floor, 250 ft below mean sea level. Low peak accelerations of the vertical component (3 - 4 milli-g's) and the combined horizontal component (20 - 28 milli-g's, Fig. 1) during this event suggested that piles would not suffer a loss of capacity. Therefore, the actual earthquake was scaled to higher magnitudes, i.e., Richter Magnitude 8.0 for the vertical component of motion, and Richter Magnitudes of 7.0, 7.5 and 8.0 for the resultant component of horizontal motion.

The earthquake scaling procedure involved (1) transforming the time history of the component of motion into the frequency domain; (2) scaling the Fourier amplitude spectrum of the original time history to match a spectrum, termed the "target spectrum" [Trifunac ([2])], that would represent a higher magnitude event (for instance, Magnitude 8.0) and (3) transforming the scaled spectrum back into the time domain while preserving the phase relationship of the unscaled (original) record to maintain the same earthquake source mechanism. The selection of the target spectrum depended upon of the level of intensity (in terms of the Modified Mercalli Intensity), distance from the epicenter, approximate soil

conditions, and direction of motion (vertical or horizontal); Original, target and scaled (computed) spectra for the combined horizontal motion (Magnitude 8.0) are shown in Fig. 2. Since the duration of significant shaking is influenced by the magnitude of the seismic event, the time segment of strong shaking was doubled (with duplicate acceleration histories) to produce a duration of strong shaking consistent with the magnitude of the target spectrum. Finally, the scaled acceleration time history (Fig. 3) was converted to a displacement time history that was used to control the motion of a pressurized test chamber into which the model pile was driven.

Testing Apparatus

A closed-loop hydraulic testing machine (Fig. 4) was used to apply the programmed seismic motion to the soil contained in a pressurized test chamber. The chamber was the largest chamber that could be accommodated by the machine: 21 inches in height and 20 inches in diameter (Fig. 5). Preliminary studies were conducted with buried accelerometers in the chamber to ensure that the shear strain amplitudes produced within the soil by the motion of the chamber within the testing machine were equal to those that would have occurred *in situ* during the simulated seismic event.

The model test pile, which was driven by impact into pressurized, submerged, very fine sand in the chamber, was a steel, closed-end cylindrical tube, 1 inch in diameter, 16 inches long, and with a wall thickness of 0.05 inches. The pile was instrumented internally with three levels of strain gages to sense axial load distribution.

Movement at the pile head was monitored by a single LVDT. Two miniature pore water pressure transducers were also buried within the chamber to sense the build-up of pore water pressure in the soil 0.5 inches (1 radius) from the wall of the pile ("near field") and 6.0 inches (12 radii) from the pile wall ("far field"). A flexible cable was attached to the head of the pile, which protruded through a port in the chamber, through which biased (static) tension load was applied continuously by means of a dead-weight-and-spring-system. The purpose of the weight-and-spring loading system was to simulate the

presence of a simple superstructure of known natural frequency, such as a floating structure, that feeds axial load back into the pile during the seismic event as the pile's motion excites the structure. The spring constant was varied so that the natural frequency of the loading system (simulated superstructure) varied from 0.1 sec to 1.0 sec. This period varied from lower than to higher than the predominant period of the simulated, time-scaled seismic event. The principal effect of superstructure feedback was to provide excursions of pile head load of (typically) 10 - 20% during shaking. During some vertical-motion-only shaking tests with high initial biased loads, these excursions were sufficient to cause pile pullout without the generation of pore water pressure within the soil.

The simulated seismic records were applied through the base of the chamber: Through vertical motion to simulate the vertical component of seismic motion, through rotary motion to simulate the resultant horizontal component, and through a combination of vertical and rotary motion to simulate the entire event.

Model to Prototype Scaling

In addition to scaling the magnitude of the earthquake upward, it was also desirable to establish geometric scaling between the model and prototype. Such scaling was then combined with the earthquake scaling to produce reasonable similitude between the model tests and the response of a pile under biased tension loading during a strong seismic event at a deep soil site. The analysis performed to establish geometric similitude rules was partially based upon the characteristic of the chamber that known effective stresses can be applied at the boundaries. This analysis included both "static" and "dynamic" components.

Static scaling rules were used to establish both a length scale, N, and values for chamber pressures. Two applied isotropic chamber pressures, 2.5 and 5.0 psi, simulated a range of depth-average, ambient horizontal effective soil stresses corresponding to pile penetrations of 20 and 40 ft, respectively ($\underline{3}$). The pressure and penetration scaling is illustrated in the following, in which L = pile penetration, σ'_h = horizontal effective stress,

m = model, p = prototype, K_o = lateral earth pressure coefficient, and γ' = buoyant unit soil weight:

Let L_p = 40 feet, and let the length scale factor N = 40;

Let σ'_h at 0.67 L_p = σ'_h at 0.5 L_m (horizontal effective stresses against the prototype and model piles at the depth of mean load transfer assuming a triangular distribution of lateral stress with depth in the prototype and a constant value in the model);

Let the prototype sand have K_{op} = 0.48; and γ' (model and prototype) = 55 pcf; then

σ'_h at 0.67 (40 ft) = 0.67 (40 ft) 55 (0.48) = 708 psf = 5.0 psi = chamber stress, and

$NL_m(0.5)(5 \text{ psi}) = L_p(0.67)(5 \text{ psi}) = 40(0.67)(5)$; from which L_m = 1.33 feet.

Since N = 40, the diameter of the prototype pile is 40 inches. A similar procedure can be followed to show that an isotropic chamber pressure of 2.5 psi and L_m = 1.33 feet (16 inches) models a 20-foot prototype pile with a diameter of 20 inches.

It was also deemed desirable to scale time and soil hydraulic conductivity characteristics in order to affect model-to-prototype similitude with respect to stress changes and pore water pressure diffusion rates during application of the modelled seismic event. It is noted that the test chamber drains only at the top surface of the sand, which was considered characteristic of prototype conditions. The choice of the scaling factor for time was conditioned simultaneously by two practical considerations: (1) the capabilities of the available closed-loop hydraulic testing machine to track the applied displacement time history, and (2) the finest soil (and lowest hydraulic conductivity) that could be found that did not possess cohesive characteristics and that could be saturated by gravity, as required by the design of the testing chamber. A mixture of a very fine sand and finely ground glass beads, termed micro-fine sand, was used as the model sand. The two time scaling factors resulting from dynamic stress and diffusion considerations were both approximately equal to 7. That is, time was compressed by a factor of 7 and accelerations were multiplied by a factor of 7. Details of time scaling are described in Ref. 3. Time scaling resulted in simulated superstructures with natural frequencies of 0.7 - 7 sec.

Using micro-fine sand (having a coefficient of permeability of 1.25×10^{-3} cm/sec) as the model sand and a time scaling factor of 7, the coefficient of permeability of the prototype soil was approximately 10^{-2} cm/sec.

During most of the tests involving only simulated vertical soil motion (Phase 1), the dynamic scaling rules were not observed. However, a few tests were conducted following these rules to verify conclusions drawn from the majority of the tests in Phase 1. In tests focusing the behavior of piles subjected to simulated horizontal motion and combined horizontal and vertical motion (Phase 2), these scaling rules were followed for all shaking tests.

TEST PROCEDURES AND RESULTS

Estimation of Static Capacity

A relation between penetration resistance during driving and static uplift capacity obtained from loading tests was derived experimentally to infer the percentile of the static capacity applied by any given biased load in the simulated seismic loading ("dynamic") tests. Dynamic tests were performed under conditions identical to those that existed in the static tests by applying the magnitude-scaled or magnitude-and-frequency-scaled displacement time histories for the selected seismic event to the soil while the pile was held under biased uplift load. For those piles that did not fail during the simulated seismic event, static loading was performed to failure after the simulated event to define the post-event capacity.

Typical Results

A total of 44 tests were conducted by varying the mode of loading, the intensity of the scaled earthquake, the magnitude of the biased static load and the natural frequency of the simulated superstructure. Time history measurements of (1) load on the pile at three locations, the pile head, at a depth of 7 in., and 1.0 in. above the pile toe, (2) pore water pressures for near and far fields, and (3) pile-head movement were made for all tests in the program. Measurements for a typical test in which the pile was completely pulled out of the

chamber during the simulated seismic event (M = 8.0, horizontal and vertical components applied) are shown in Figs. 6 - 8. The time scale shown is the actual test time. In a prototype the time values would be multiplied by 7. In that test, the loss of capacity produced by the generation of excess pore water pressure coupled with the dynamic load excursion on the pile head of about 10 per cent of the static bias combined to produce complete and catastrophic failure just at the completion of shaking. Liquefaction (manifested physically by sand boiling) took place about two seconds after completion of the simulated seismic event (14 seconds in the prototype).

The failure mechanism of the pile during an event with strong horizontal shaking can be explained as follows. Shearing strains in the soil generated primarily by the sudden repetitive pullouts of the pile (in response to the superstructure feedback), and additional shearing strains in the soil generated by the horizontal component of the seismic event induced build-up of pore water pressures in the soil to a level high enough to promote significant degradation of skin friction through reduction of effective normal stresses and to allow the pile to displace upward. This action occurred before liquefaction could occur in the free field. Evidence exists that failure started at or near the toe of the pile and progressed rapidly up the pile. Once the pile moved significantly upward, the effective stress in the soil beneath the toe was reduced to the point at which the soil liquefied under the toe, and liquefaction spread rapidly into the mass of soil around the pile. This occurrence has important implications relative to potential rapid progressive failure in pile groups, particularly where the piles are short.

It is noteworthy that no failures were observed under a purely vertical component of loading unless the static biased load plus the feedback load from the superstructure became equal to the static uplift capacity of the pile. This observation is consistent with the observation that no excess pore water pressures developed prior to pullout failure in the vertical-motion-only tests. Therefore, the horizontal component of motion is by far the most destructive.

INTERPRETATION

Pile Behavior During Seismic Event

Based on the experimental results, interpreted contour plots were developed for stability conditions (sustained load and small pile movement), mobility conditions (sustained load associated with substantial pile movement) and failure conditions (total loss of pile capacity) for a displacement pile driven in medium dense submerged sand with a coefficient of permeability of 10^{-2} cm/second, loaded with a biased tension load, and subjected to a simulated seismic event that occurred 45 mi. (74 km) from the earthquake epicenter (Figs. 9 - 11). In these plots, the number in parentheses represents the total measured (unscaled) pile movement during shaking. By inspection of all static tests, it was judged that a pile movement of 0.007 in. (movement of 0.05 in. in the prototype based on a dynamic scaling factor of 7) represented an upper bound to ensure pile stability, and piles that moved less than that amount vertically were judged stable. Movement in excess of 0.007 in. but less than total extraction represented a "mobility" condition between stability and complete failure. Based on this criterion, the contour lines separating stability and mobility conditions were drawn. The contour line between failure and mobility conditions was simply drawn by joining approximately the points in the plot in which failure was visually observed, applying judgment in recognition of the coarseness of the grid.

The effect of distance between the pile site and event epicenter on stability and mobility conditions is also considered in Fig. 12, which applies to a relative density of 55% and chamber pressure of 2.5 psi (simulated toe depth of 20 ft). Ratios of peak ground accelerations for distances of 15 mi. (25 km) and 30 mi. (50 km) to peak ground accelerations for the distance of 45 mi. (74 km), e.g., $a_g^{25\ km} / a_g^{74\ km}$ [using the predictive attenuation equation proposed by Joyner and Boore (4)] were used to multiply the measured pile movements given in Fig. 9. The criterion of maximum pile movement of 0.007 in. to ensure pile stability was then used to define the contour line between stability and mobility conditions.

Post-Event Pile Capacity

The results of static uplift tests conducted to failure after the simulated seismic event on piles that did not fail after being subjected to horizontal or combined motion are summarized in Fig. 13. Included in that figure are the results of tests conducted at initial soil relative density of 55%. It is obvious that the strong motion produced a permanent loss of capacity that varied from very minor (M = 7) to very significant (M = 8 with loads above 60% of static capacity).

DESIGN INFERENCES

Figures 9 - 12 suggest a design hypothesis for piles for ordinary conditions at medium dense sand sites in which the superstructure is not assumed to be ductile, which is a superstructure that will fail if an individual pile fails. For piles under biased tension loads that anchor superstructures having fundamental periods near the fundamental period of seismic motion, it is desirable to maintain a "stability" condition.

For stability of short piles ($\leq$ 20 ft in length) or for the upper 20 ft of longer piles, it is suggested that the static biased load plot on or to the left of the appropriate contour line in Fig. 12, since the chamber pressure of 2.5 psi simulates mean effective stresses over the top 20 ft of the soil profile. For example, if the design event is of Richter Magnitude 7.75 and the epicentral distance is 50 km, it is observed in Fig. 12 that the stable static biased load that can be sustained is 60% of the static uplift capacity of the pile. Stated in other terms, the pile should be designed for a factor of safety against pullout of 1/0.60 = 1.67, provided other factors, such as hydraulic loading simultaneous with seismic loading, are not significant.

For piles 40 ft long (or the upper 40 ft of longer piles) and for D_r = 70% it was not possible to develop contours of stability-mobility for varying epicentral distances, since not enough tests were conducted at high biased loads in the chamber when a 5 psi confining pressure or a relative density of 70% was employed. However, one can use Figs. 10 and 11 to ascertain the permissible static biased load for a 45 mi. (74 km) epicentral distance (or

greater). These figures indicate stability for all Richter Magnitudes up to 8 provided that the factor of safety against static uplift capacity is 1.33 or higher. Because this value is less than the minimum factor of safety of 1.5 normally assumed for static or quasi-static conditions, at this epicentral distance earthquake conditions would not control the design. Further research is clearly needed at smaller epicentral distances in medium dense sands, for longer piles and for non-displacement piles.

Phenomenologically, it is clear from a comparison of Figs. 10 and 11 that the pile foundation of a biased-tension-loaded bridge or hydraulic structure should consist of fewer, longer piles, rather than more, shorter piles to develop the maximum resistance to pullout failure during earthquakes.

This design hypothesis is based on the assumption that the magnitude of the structural feedback forces have been modelled correctly in this study for a particular case. This will have been correct only if the superstructure behaves as a simple mass-spring system that responds only to the vertical motion of the pile. Other sources of dynamic superstructure loading, such as wave and inertial loadings, may cause the magnitude of pile loading to be different from the simple feedback loading reproduced in these experiments. In the absence of information on this effect, it is suggested that the factor of safety be applied not to the static biased load but rather to the sum of the static biased load and the peak dynamic load applied to the pile by the superstructure during the seismic event.

CONCLUSIONS

The following conclusions have been drawn from this study:

(1) For the earthquake studied, the capacity of the soil to sustain applied uplift loads from a driven displacement pile was not substantially affected by the action of the vertical component of the simulated seismic event. However, the pile motion produced feedback in the simple mass-spring structure to which it was attached, which periodically increased the load on the pile during the simulated event. Additional loading as a result of superstructure

feedback produced failure for the case of applied high biased loads (90% of the pile's static capacity).

(2) When the combined horizontal component of motion was added, both stuperstructure feedback and increased pore water pressures developed, resulting in the behavior described in Figs. 9 - 12.

(3) The capacity of the soil to sustain static uplift loads after the seismic event was not affected significantly by the action of the horizontal component of a Magnitude-7.0 event. Reductions in capacity occurred in stronger events, however, as shown in Fig. 13.

(4) The interaction of the soil and overlying water was not investigated experimentally in this study. For deep water sites, futher loss of capacity may occur due to pore water pressure buildup from this effect.

ACKNOWLEDGMENTS

REFERENCES

1. Sleefe, G.E., and Engi, D., "Seafloor Response for Two Southern California Earthquakes," in Proceedings, 1987 SEM Spring Conference on Experimental Mechanics, Houston, Texas, pp. 747-753.

2. Trifunac, M.D., " Preliminary Empirical Model for Scaling Fourier Amplitude Spectra of Strong Acceleration in Terms of Modified Mercalli Intensity and Recording Site Conditions," Earthquake Engineering and Structural Dynamics, Vol. 7, 1979, pp. 63-74.

3. O'Neill, M. W., Vipulanandan, C., and Ochoa, M., "Response of Tension Piles to Simulated Seismic Motion in Saturated Fine Sand," <u>Report No. UHCEE-90-09</u>, Department of Civil and Environmental Engineering, University of Houston, 286 pp.

4. Joyner, W.B., and Boore, D.M., " Measurement, Characteristics and Prediction of Strong Ground Motion," State-of-the-Art Report, in <u>Proceedings</u>, Specialty Conference on Earthquake Engineering and Soil Dynamics II, ASCE, June, 1988, pp. 43-102.

5. Poulos, H.G., "Influence of Cyclic Loading on Axial Pile Response," in <u>Proceedings</u>, Second International Conference on Numerical Methods in Offshore Piling, ICE and The University of Texas, Austin, Texas, April, 1982, pp. 419-440.
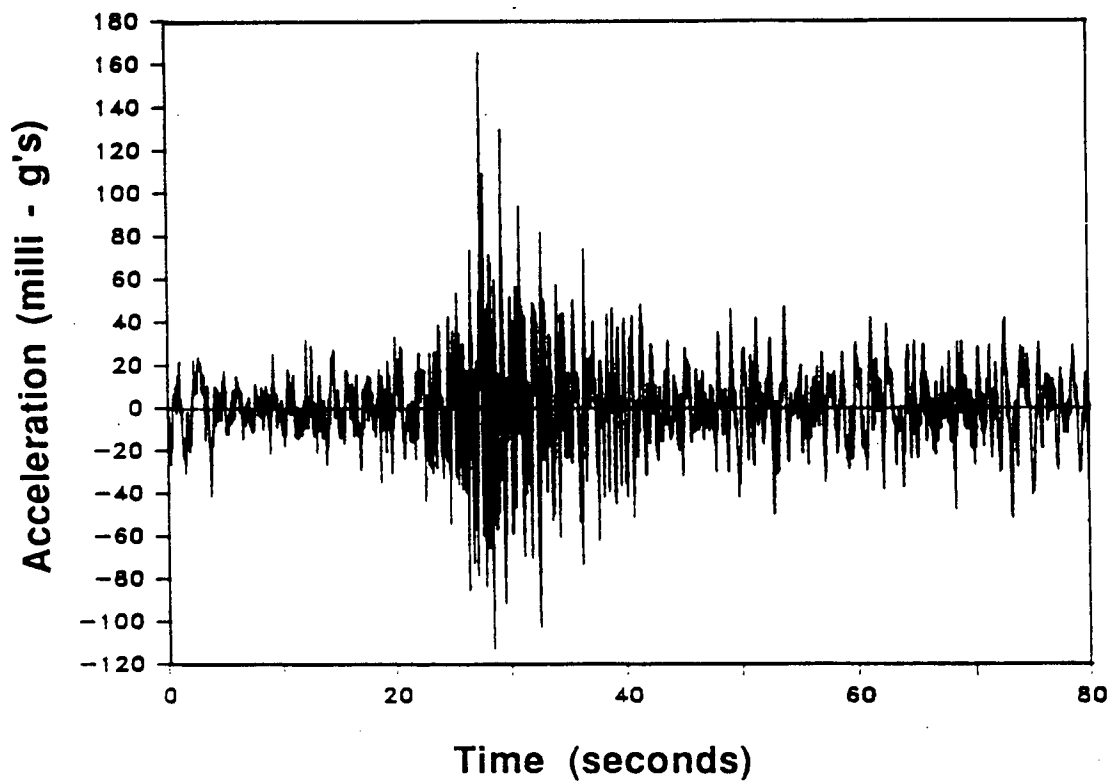
Fig. 1. Combined X and Y Components of Oceanside Earthquake (M = 5.8) of July 13, 1986.

Fig. 2. Original, Target and Computed (Scaled, M = 8.0) Spectra (Horizontal Motion) of Oceanside Earthquake.

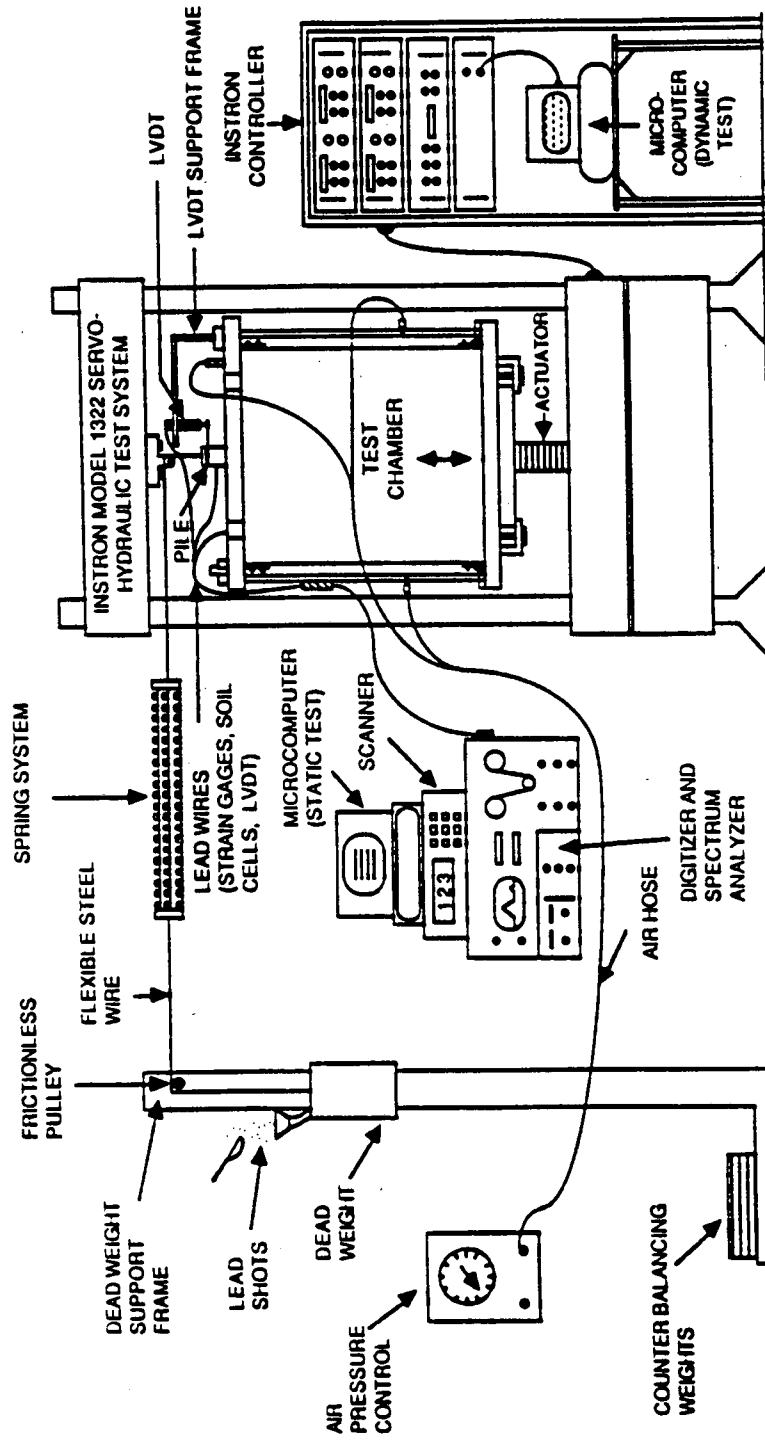Fig. 3. Combined Scaled (M = 8.0) Horizontal Record of Oceanside Earthquake.

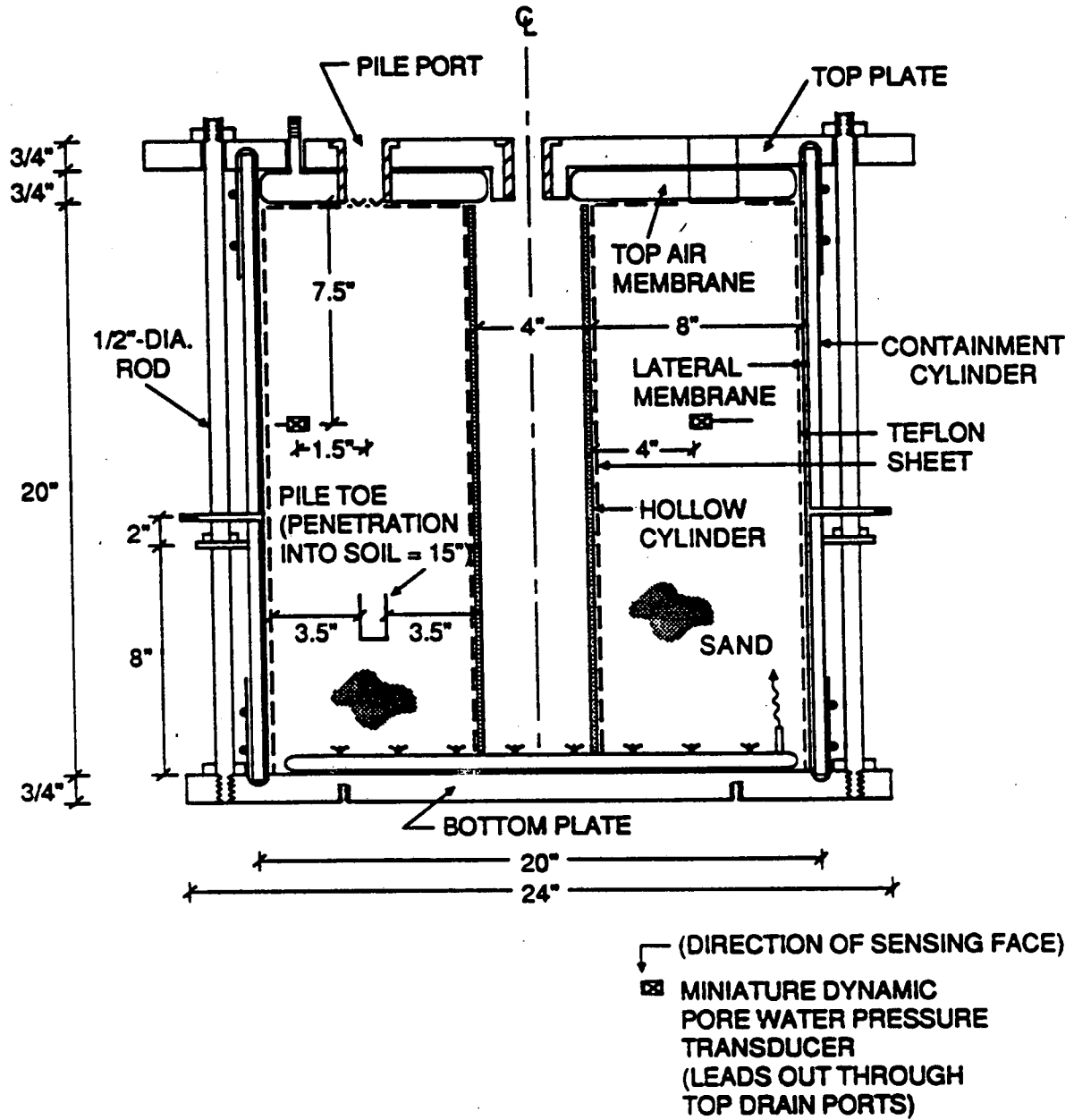Fig. 4. Schematic of Overall Testing Arrangement.

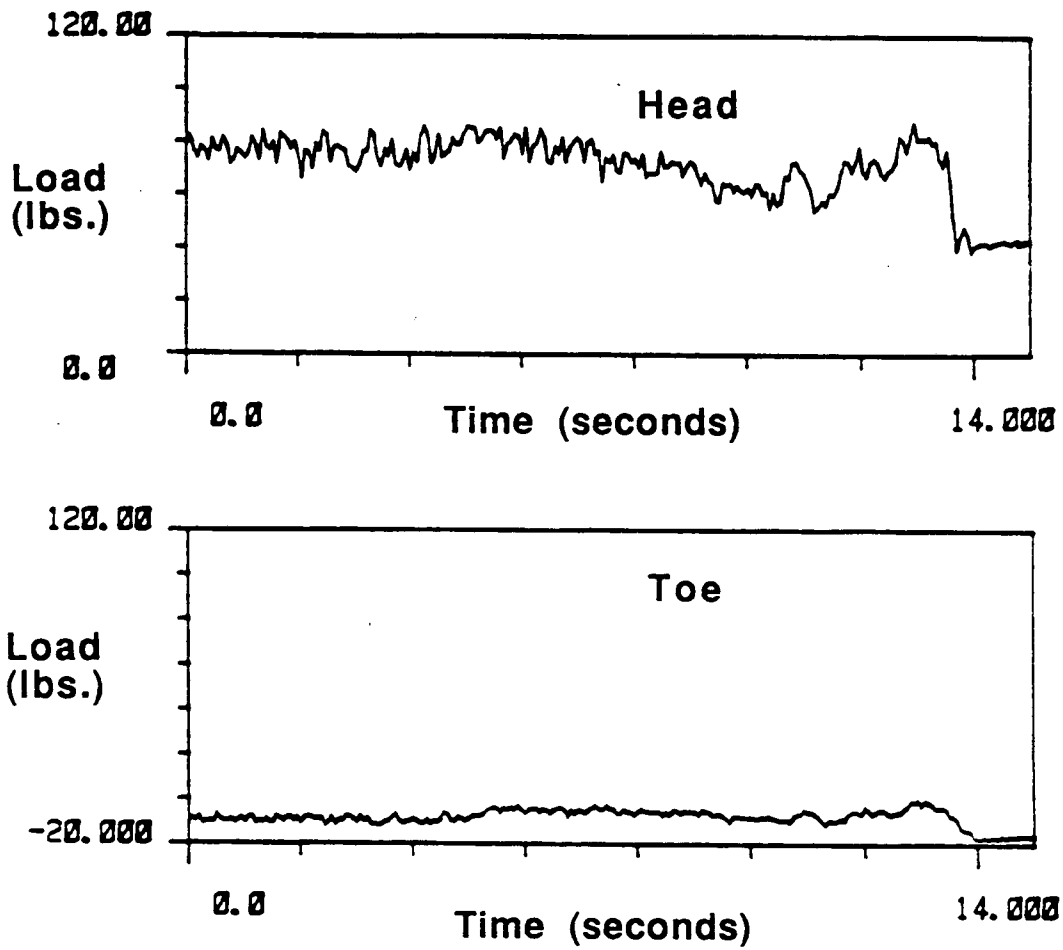Fig. 5. Schematic Elevation of Test Chamber (Rotational Motion).

Fig. 6. Time History Measurements of Dynamic Load on Pile of a Typical Test.
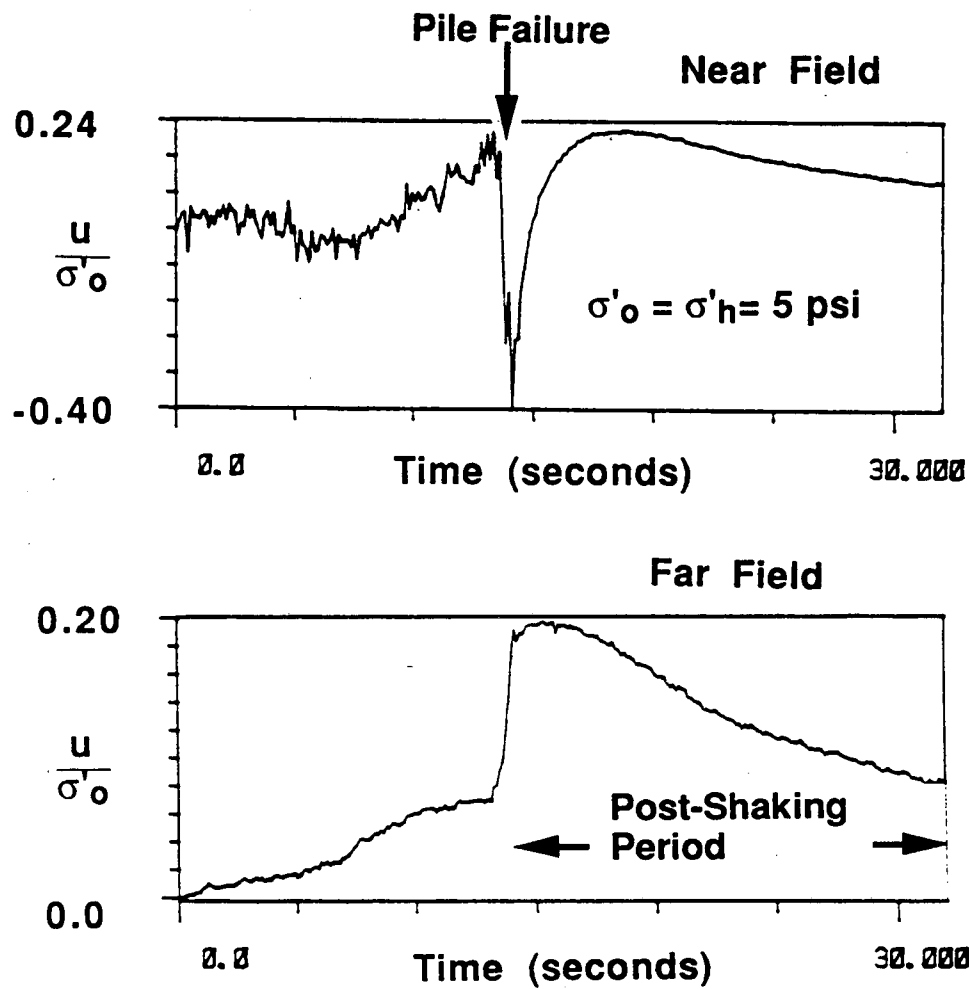
Fig. 7. Time History Measurements of Near and Far Field Pore Water Pressures of a Typical Test.
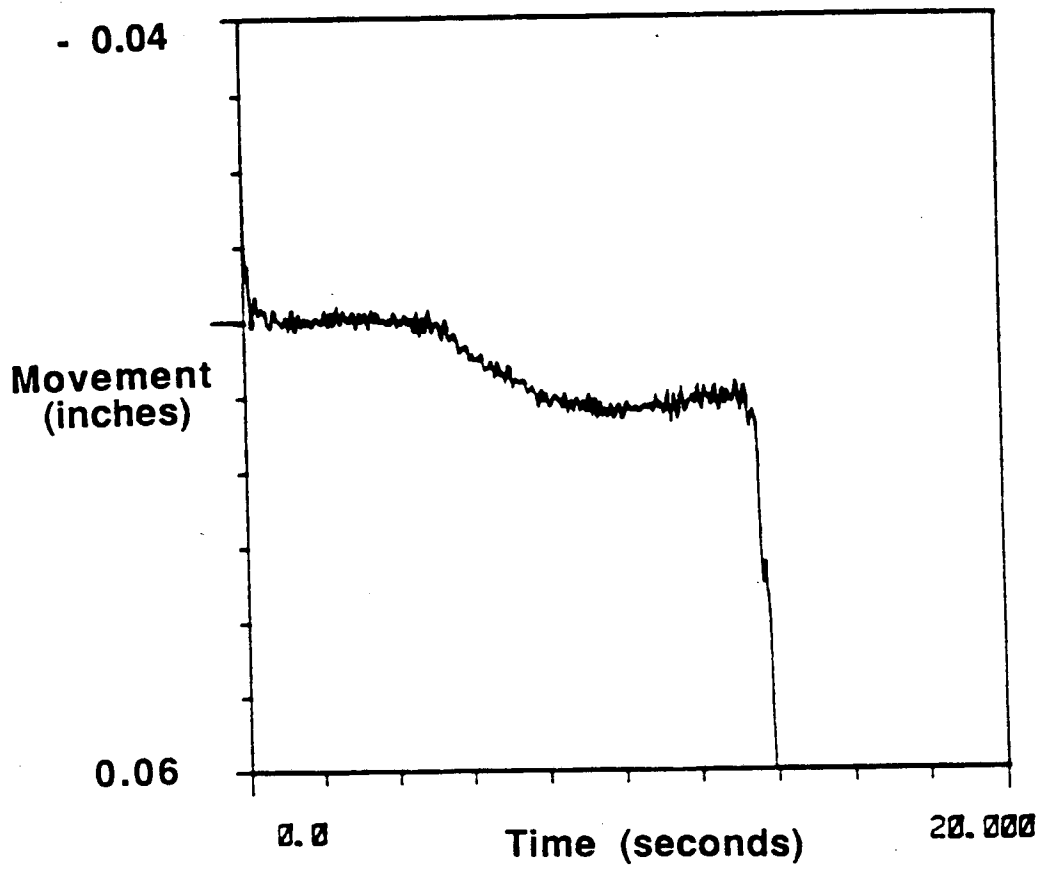
Fig. 8. Time History Measurements of Pile Head Movement of a Typical Test.
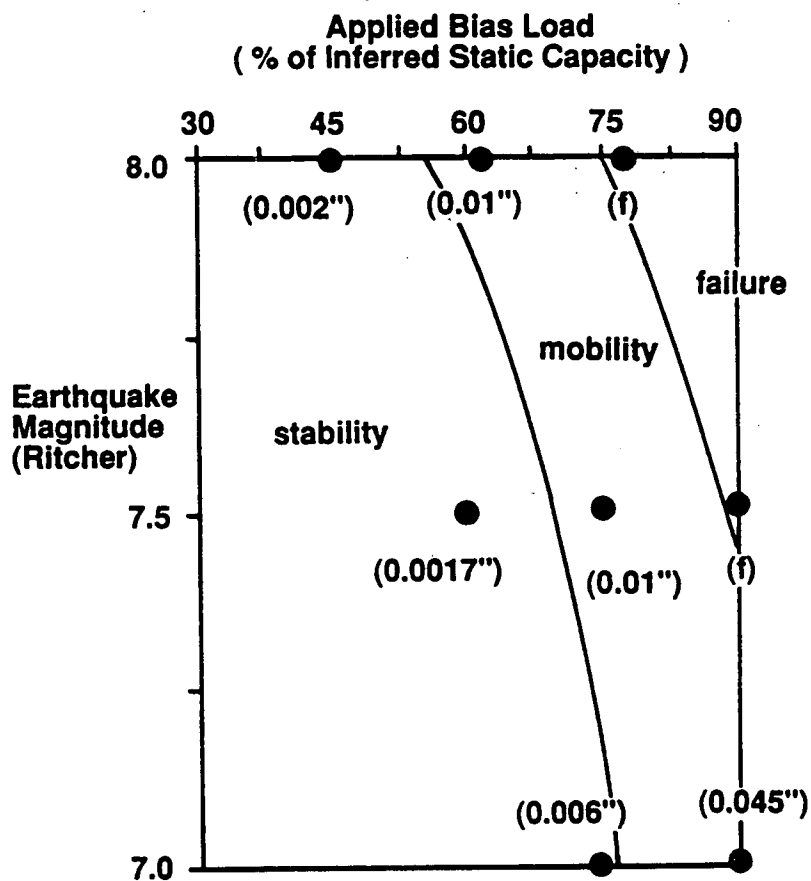
Fig. 9. Stability, Mobility and Failure Conditions; Horizontal Loading; Confining Pressure: 2.5 psi; Epicentral Distance: 74 km; Relative Density: 55%.

Fig. 10. Stability and Mobility Conditions; Horizontal Loading; Confining Pressure: 5 psi; Epicentral Distance: 74 km; Relative Density: 55%.

Fig. 11. Stability and Mobility Conditions; Horizontal Loading; Confining Pressure: 2.5 psi; Epicentral Distance: 74 km; Relative Density: 70%.

Fig. 12. Stability and Mobility Contours for Variable Epicentral Distance.

Fig. 13. Loss of Static Capacity Following Strong Ground Motion (Relative Density = 55%)

Fig. 1. Combined X and Y Components of Oceanside Earthquake (M = 5.8) of July 13, 1986.

Fig. 2. Original, Target and Computed (Scaled, M = 8.0) Spectra (Horizontal Motion) of Oceanside Earthquake.

Fig. 3. Combined Scaled (M = 8.0) Horizontal Record of Oceanside Earthquake.

Fig. 4. Schematic of Overall Testing Arrangement.

Fig. 5. Schematic Elevation of Test Chamber (Rotational Motion).

Fig. 6. Time History Measurements of Dynamic Load on Pile of a Typical Test.

Pile Failure

Near Field

0.24

$\frac{u}{\sigma'_o}$

$\sigma'_o = \sigma'_h = 5$ psi

-0.40

0.0 **Time (seconds)** 30.000

Far Field

0.20

$\frac{u}{\sigma'_o}$

← Post-Shaking Period →

0.0

0.0 **Time (seconds)** 30.000

Fig. 7. Time History Measurements of Near and Far Field Pore Water Pressures of a Typical Test.

Fig. 8. Time History Measurements of Pile Head Movement of a
        Typical Test.

Fig. 9. Stability, Mobility and Failure Conditions; Horizontal Loading; Confining Pressure: 2.5 psi; Epicentral Distance: 74 km; Relative Density: 55%.

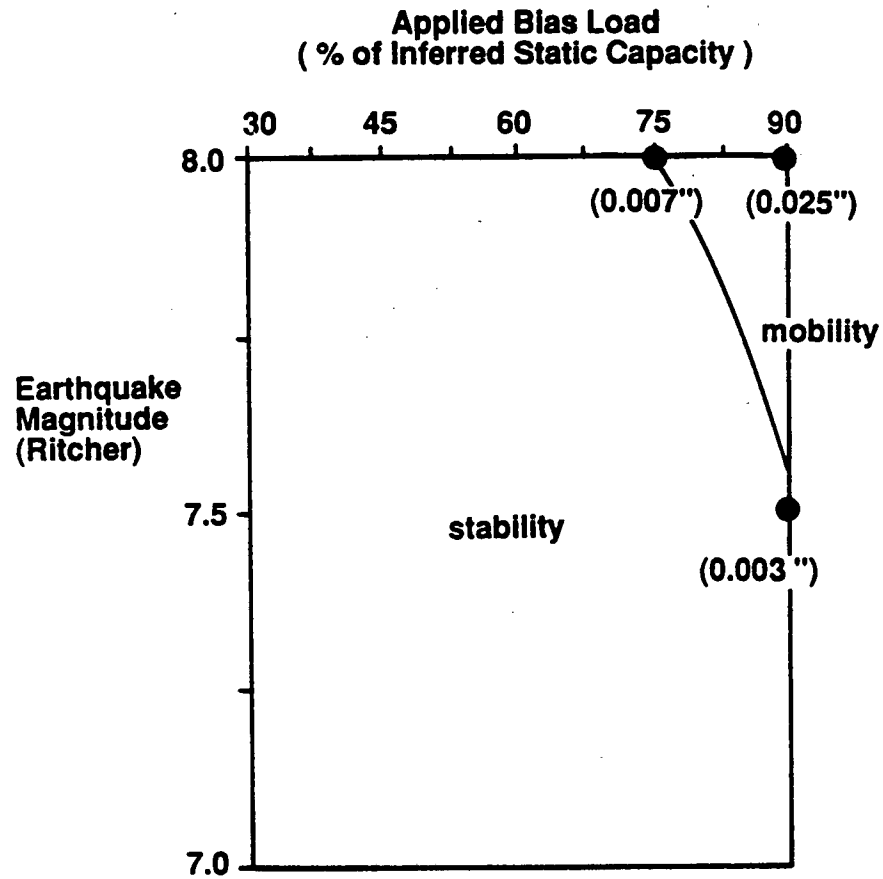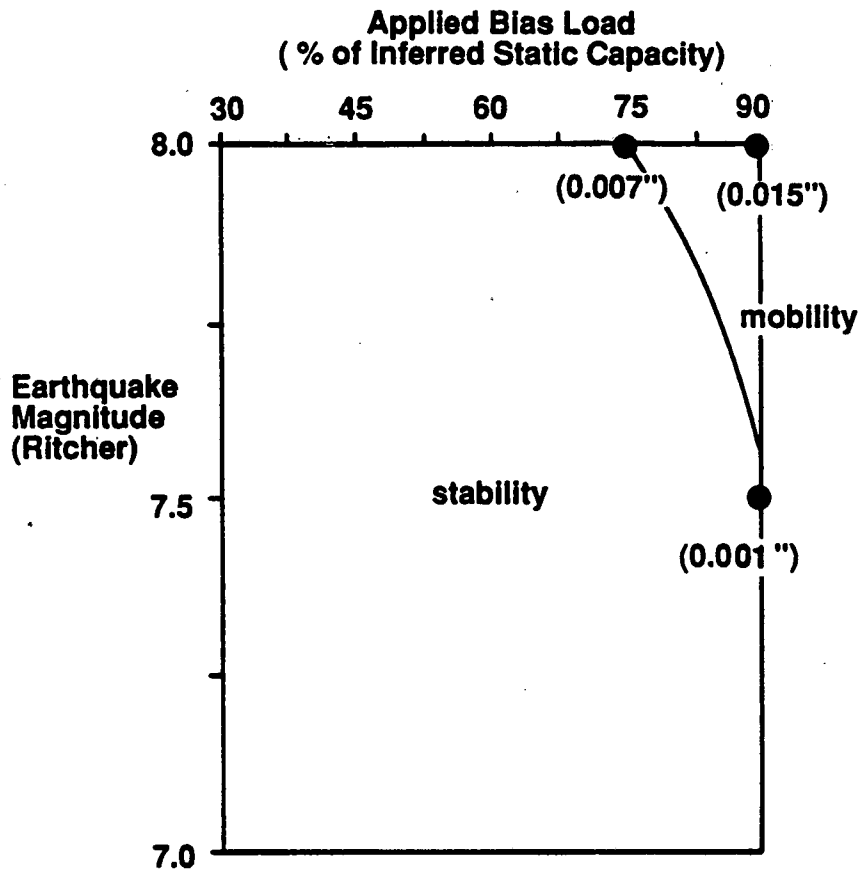**Applied Bias Load**
(% of Inferred Static Capacity)

Fig. 10. Stability and Mobility Conditions; Horizontal Loading;
Confining Pressure: 5 psi; Epicentral Distance: 74 km;
Relative Density: 55%.

Fig. 11. Stability and Mobility Conditions; Horizontal Loading; Confining Pressure: 2.5 psi; Epicentral Distance: 74 km; Relative Density: 70%.
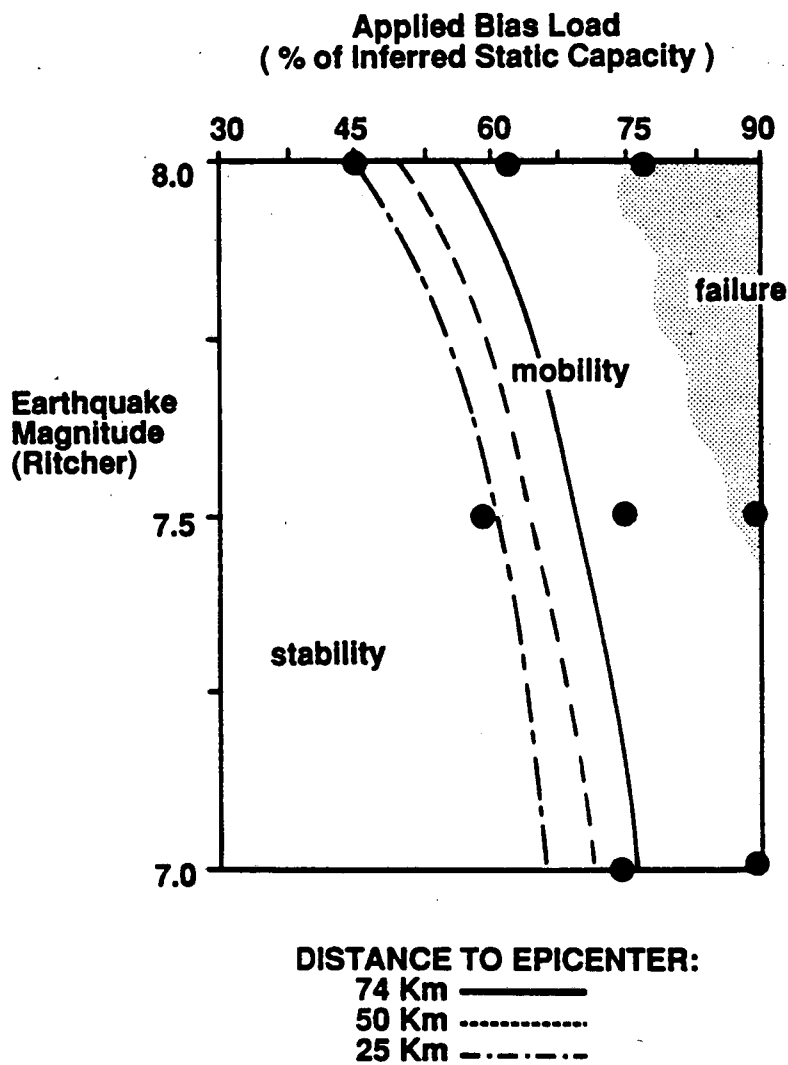
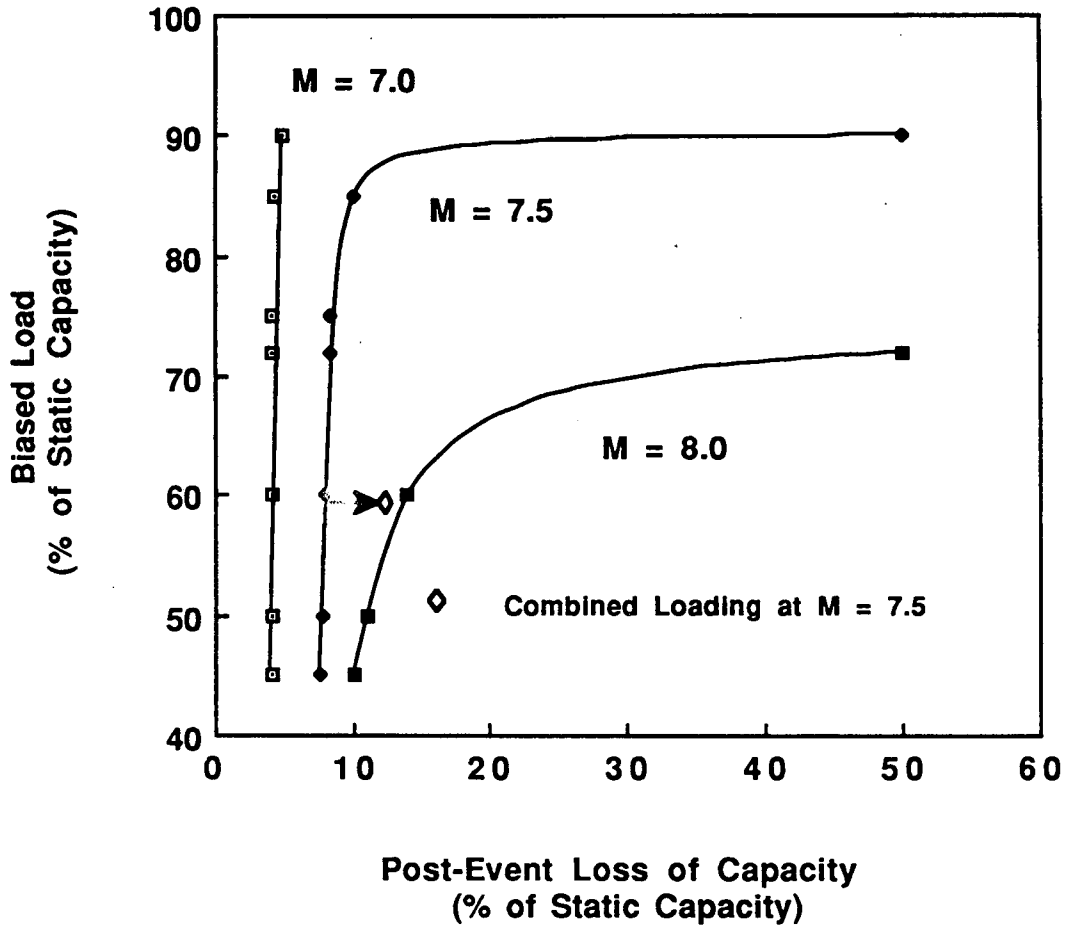Fig. 12. Stability and Mobility Contours for Variable Epicentral Distance.

Fig. 13. Loss of Static Capacity Following Strong Ground Motion
(Relative Density = 55 %)